J. Fluid Mech. (2006), *vol.* 566, *pp.* 377–388.
doi:10.1017/S0022112006002369 Printed in the United Kingdom

Nonlinear global instability in buoyancy-driven boundary-layer flows

By J. TAO

Institute of Physics, Bayreuth University, Bayreuth 95440, Germany
LTCS *and* Department of Mechanics and Engineering Science,
Peking University, Beijing 100871, China

(Received 12 March 2006 and in revised form 28 April 2006)

Direct numerical simulation (DNS) and a linear analysis of the global instability of a buoyancy layer have been performed. The spatially developing basic flow under consideration is induced by a vertical heated flat plate immersed in a thermally stratified medium. It is revealed numerically that, depending on the modified Grashof number, the disturbed flat-plate boundary-layer flows may not relax to the basic state but instead oscillate with an intrinsic frequency. The front of globally unstable waves in numerical simulations agrees very well with the position of marginal absolute instability, and the dominant frequencies in the oscillating region are identical and tuned to the marginal absolute frequency derived from the local linear dispersion relation based on the unperturbed basic state. The front of the nonlinear global modes is thus of a pulled type in this buoyancy-driven flow system.

1. Introduction

Depending on their responses to inflow impulses, spatially developing shear flows may behave as noise amplifiers or as oscillators, which are intrinsically related to the convective/absolute nature of the linear instability. It is well-established that when a flow is absolutely unstable in a finite region, such as counterflow mixing layers, hot jets and wakes, self-sustained resonances or global modes tuned at a well-defined frequency may occur (see Huerre 2000, for a review). Both kinds of flow exhibit strong nonlinearities. The objective of the present investigation is to determine the fully nonlinear global mode properties of the boundary-layer flow over a flat plate, which is immersed in thermally stratified medium.

Two essential features of global modes are the selection of the front and the global frequency. Several principles have been proposed to reveal the relationship between the global frequency and the local absolute frequency $\omega_0(X)$ (Koch 1985; Monkewitz & Nguyen 1987; Couairon & Chomaz 1997*a*, *b*, 1999*a*, *b*; Pier *et al.* 1998) An absolutely unstable flow is characterized by $\omega_{0,i}(X) = \mathrm{Im}\omega_0(X) > 0$ for weakly non-parallel flows (Briggs 1964; Bers 1983), where perturbations are not swept away from the source as in convectively unstable flows, but grow *in situ* and lead to a trailing front at some upstream position. Dee & Langer (1983) found that the front, separating the basic state upstream from the finite-amplitude state downstream, moves at the speed of the edge of the linear wave packet. This kind of front has been referred to as a pulled front (Chomaz 2003, 2005). Couairon & Chomaz (1997*a*, *b*, 1999*a*, *b*) analysed Ginzburg–Landau-type equations in a semi-infinite domain and showed that the nonlinear global mode occurs as soon as the

medium is nonlinearly absolutely unstable, and the selected frequency at threshold is the absolute frequency. In an infinite domain the steep global mode, a nonlinear global mode described by Pier *et al.* (1998), also obeys a marginal criterion: the global mode is triggered at the upstream boundary of the linear absolutely unstable domain and the global frequency coincides with the real absolute frequency at the boundary.

For a parallel flow, Delbende & Chomaz (1998) have shown numerically that the front separating the von Kármán saturated street from the unperturbed upstream wake is a pulled front. For real spatially developing flows, Pier (2002) studied the frequency selection criterion of vortex shedding in cylinder wakes and obtained a good agreement between the numerical simulation and the marginal absolute frequency calculated on the basis of the mean flow. The self-sustained oscillation frequency in the separated boundary layer flow over a double-bump geometry as computed by Marquillie & Ehrenstein (2003) was predicted well by the marginal absolute frequency, where mean velocity profiles were used for the local stability analysis. However, it is not helpful to identify the mechanism, i.e. the unstable modes governed by the linear absolute instability at the pulled front, when the mean velocity profile but not the undisturbed basic flow is used in an analysis, because nonlinear effects have been partially included in the profile.

For a flat-plate boundary-layer flow, Gaster & Grant (1975) have shown that the impulse response of the Blasius boundary layer was convected downstream, so the primary Tollmien–Schlichting modes are unambiguously convectively unstable. According to Koch's (2002) analysis, both the three-dimensional wave packet for primary crossflow vortices and the two-dimensional wave packet of high-frequency secondary instability were found to be convectively unstable as well. Recently, Brandt *et al.* (2003) showed numerically that the secondary streak instability of boundary-layer flow is also convective in nature.

When the flow is driven by buoyancy, however, Krizhevsky, Cohen & Tanny (1996) have shown that the flow changed from convectively unstable to absolutely unstable at a critical Grashof number G_{ca}, which increases with the Prandtl number. Tao, Le Quéré & Xin (2004*a*) extended the spatio-temporal analysis by providing a more general basic flow solution for a buoyancy-driven boundary layer immersed in a thermally stratified medium. Based on this solution, a finite absolutely unstable domain was found in the downstream direction, defined by two critical Grashof numbers G_{ca} and G_{ac} where the convective–absolute and absolute–convective instability transitions occur. Such kinds of flow are called type 'AF' by Monkewitz & Sohn (1986), meaning absolutely unstable flow with a free boundary. The buoyancy-driven or natural–convection boundary-layer flow is a basic model for solar heating systems or mountain winds (Prandtl 1952). It is also an appropriate model to study the non–linear global instability: it is a weakly non-parallel flow, and the marginal linear absolute frequency can be obtained directly by analysing the basic flow solution. Though substantial progress in the understanding of global instability has been made recently (for a review see Chomaz 2005), to the best of our knowledge, the front and global frequency selection criteria for flat-plate boundary-layer flows have not yet been identified, which is the motivation for the present work.

The paper is organized as follows. In § 2 the numerical solution procedure is described. The basic flow and linear theory are briefly outlined in § 3. The nonlinear global mode supported by the spatially developing basic flow is documented in § 4, as computed by direct numerical simulation of the coupled Navier–Stokes and energy equations. The corresponding front selection criterion and the global frequency

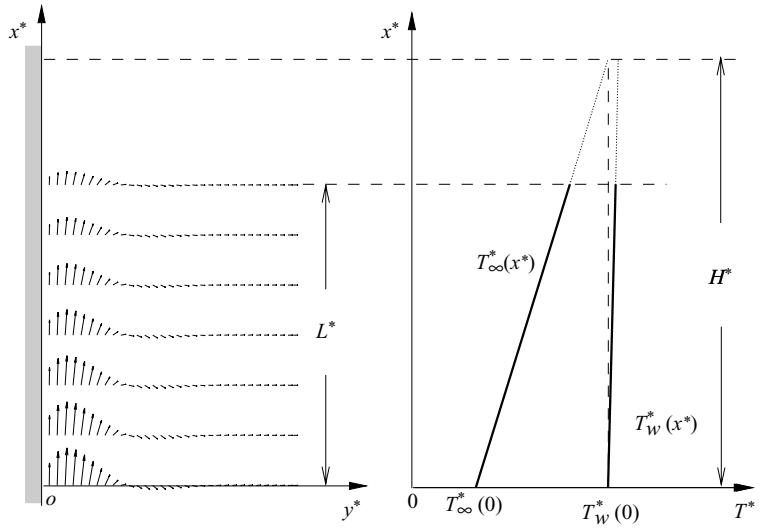

FIGURE 1. Sketch of a buoyancy-driven flow near a vertically heated flat plate, which is immersed in a thermally stratified medium.

selection criterion of the global mode are discussed. Finally, some conclusions are drawn in § 5.

2. Geometry and governing equations

The boundary layer to be considered here is shown in figure 1. The temperature at the vertical heated wall $T^*_w(x^*)$ and in the ambient fluid $T^*_\infty(x^*)$ vary linearly in the downstream direction,

$$T^*_w(x^*) = T^*_w(0) + N_w x^*,\ T^*_\infty(x^*) = T^*_\infty(0) + N_\infty x^*,\ T^*_w(0) - T^*_\infty(0) = \Delta T^*(0) > 0.$$

N_w and N_∞ are the temperature gradients at the wall and in the medium. The coordinate x^* is measured vertically and opposite to the direction of acceleration due to gravity g, and y^* is the coordinate normal to the surface (stars indicate dimensional quantities). The subscript ∞ denotes the ambient condition, and $\Delta T^*(0)$ is the temperature difference between the wall and the background fluid at $x^* = 0$.

In order to obtain a stable thermally stratified medium, we assume $N_\infty > 0$ and $N_w \geqslant 0$. H^* is a characteristic length with $T^*_\infty(H^*) = T^*_w(0)$. L^* is the length of the computational domain used in the numerical simulations. The Grashof number, the Prandtl number and other non-dimensional parameters, namely temperature, lengths, time and pressure, are defined as

$$Gr = \left(\frac{g\beta\Delta T^*(0)H^{*3}}{\nu^2}\right)^{1/4},\quad Pr = \frac{\nu}{\kappa},\quad \Phi = \frac{T^* - T^*_\infty(x^*)}{T^*_w(x^*) - T^*_\infty(x^*)},$$

$$(X, Y, H, L) = \frac{Gr}{H^*}(x^*, y^*, H^*, L^*),\quad \tau = \frac{\tau^*\nu Gr^3}{H^{*2}},\quad P = \frac{[P^* - P^*_\infty(x^*)]H^{*2}}{\rho\nu^2 Gr^4},$$

where ρ, ν, κ and β are the fluid density, the kinematic viscosity, the thermal diffusivity and the coefficient of thermal expansion.

By applying the Boussinesq approximation, we obtain the following governing dimensionless equations for the perturbations u, v, ϕ and p:

$$\left.\begin{aligned}
&\frac{\partial u}{\partial \tau}+\frac{\partial(uu+2uU_0)}{\partial X}+\frac{\partial(vU_0+uV_0+uv)}{\partial Y}=-\frac{\partial p}{\partial X}+\frac{1}{Gr}\nabla^2 u+\frac{1}{Gr}\phi[1+(a-1)\varepsilon X],\\
&\frac{\partial v}{\partial \tau}+\frac{\partial(vU_0+uV_0+uv)}{\partial X}+\frac{\partial(2vV_0+vv)}{\partial Y}=-\frac{\partial p}{\partial Y}+\frac{1}{Gr}\nabla^2 v,\\
&\frac{\partial \phi}{\partial \tau}+\frac{\partial(\phi U_0+u\phi)}{\partial X}+\frac{\partial(V_0\phi+v\phi)}{\partial Y}=\frac{1}{GrPr}\nabla^2\phi-\frac{u[1+(a-1)\phi]}{Gr[1+(a-1)\varepsilon X]}\\
&\qquad\qquad+\frac{2(a-1)}{PrGr^2[1+(a-1)\varepsilon X]}\frac{\partial\phi}{\partial X}-\frac{(a-1)(U_0\phi+u\phi_0)}{Gr[1+(a-1)\varepsilon X]},
\end{aligned}\right\} \tag{2.1}$$

where the operator $\nabla^2=\partial^2/\partial X^2+\partial^2/\partial Y^2$, $a=N_w/N_\infty$, and $\varepsilon=1/Gr$. $(a-1)\varepsilon$ characterizes the degree of spatial inhomogeneity of the basic flow. $U=U_0+u$, $V=V_0+v$, $P=P_0+p$ and $\Phi=\phi_0+\phi$, where U_0, V_0, P_0 and ϕ_0 constitute the undisturbed basic flow solution which will be determined in § 3.

The governing equations are solved by a semi-implicit projection method (Chorin 1967; Peyret & Taylor 1990) on a uniform mesh. The most time-consuming part of the solver, the solution of the corresponding discrete Poisson's equation, is obtained by a multigrid method. The spatial discretization of the primitive variables uses a finite difference scheme and a partially staggered approach or ALE (arbitrary Lagrangian Eulerian) method: the pressure P and temperature Φ are defined at the cell centre while both components of the Cartesian velocity u and v are defined at the cell corner. This method is convenient for application of the buffer domain technique that is discussed below.

The boundary conditions are as follows. The homogeneous Dirichlet boundary condition ($u=v=\phi=0$) is imposed at the inlet. On the solid wall a no-slip boundary is used, and at the far field homogeneous Neumann boundary conditions are applied:

$$\frac{\partial u}{\partial Y}=\frac{\partial v}{\partial Y}=\frac{\partial \phi}{\partial Y}=0. \tag{2.2}$$

At the outflow boundary, vanishing second derivatives in the X-direction for the disturbing velocities u, v and ϕ are used. For the pressure, Neumann boundary conditions are used at the inlet and on the solid wall. A zero second derivative in the Y-direction is used at the far field and a zero third derivative of the pressure in the X-direction is used at the outlet boundary.

A buffer domain technique is used to eliminate the possible reflection of waves near the outlet, which has been used by Chomaz (2003) to study the nonlinear dynamics of parallel wakes. The total computational domain includes an original domain (length L) and a buffer domain (length $\delta_r+\delta_f$). A linear damping term $-A(X)u(X,Y,\tau)$ is added to equation (2.1) for the u component, and the same treatment is applied to the velocity v and temperature ϕ. The damping function $A(X)$ is smooth and given by the (Högberg & Henningson 1998)

$$A(x)=\begin{cases}0, & X<L,\\ A\Big/\left[1+\exp\left(\dfrac{\delta_r}{X-L}+\dfrac{\delta_r}{L+\delta_r-X}\right)\right], & L<X<L+\delta_r,\\ A, & L+\delta_r<X<L+\delta_r+\delta_f.\end{cases}$$

The damping intensity is determined by A, δ_r is the length of the region where the damping grows from zero to A, and δ_f is the length of the region where the damping intensity is kept constant.

It has been verified that the global frequencies do not change for values of the damping coefficient A between 0.2 and 5. $A = 0.5$ is used in all simulations. The buffer domain occupies a seventh of the total computational domain. The total grid varies from 576× 96 to 1024× 96 with the original domain from $L = 60$ to $L = 100$, and $Y_{max} = 12\sqrt{2}$ is used in all simulations.

The initial divergence-free perturbation used in the simulations corresponds to a vortex with a Gaussian envelope. Its streamfunction is

$$\psi' = \delta \exp\left(-\frac{(X - X_0)^2 + (Y - Y_0)^2}{r_0^2}\right) \tag{2.3}$$

with (X_0, Y_0) the centre of the vortex, δ the strength parameter of the vortex and r_0 the initial size of the perturbation.

3. Basic flow and linear theory

In order to obtain a similarity solution, Gebhart's method (Gebhart *et al.* 1988) is used to find the following forms of velocities and temperature:

$$U_0 = 2[1 + (a-1)\varepsilon X]F_0'(\eta), \quad V_0 = 2\sqrt{2}(1-a)\varepsilon F_0(\eta), \quad \phi_0(X, Y) = H_0(\eta) \tag{3.1}$$

where $\eta = Y/\sqrt{2}$. Note that η does not include X because of the background thermal stratification; this is different from the forced-convection boundary layer described by the Blasius equation.

By applying the boundary-layer approximation and the above transformations, we can obtain the following ordinary differential equations for steady basic flow:

$$\left.\begin{aligned} &F_0''' + 4(a-1)F_0F_0'' - 4(a-1)(F_0')^2 + H_0 = 0, \\ &\frac{1}{Pr}H_0'' + 4(a-1)F_0H_0' - 4F_0'[1 + (a-1)H_0] = 0, \end{aligned}\right\} \tag{3.2}$$

with boundary conditions

$$F_0(0) = F_0'(0) = 1 - H_0(0) = F_0'(\infty) = H_0(\infty) = 0. \tag{3.3}$$

A no-slip boundary condition for the velocity is used on the wall, while in the far field the vertical velocity decays.

It has been confirmed by direct numerical simulations (Tao, Le Quéré & Xin 2004*b*) that this similarity solution describes exactly the steady convection flows near the vertical walls dissipating uniform heat flux in a cavity. Since the velocity component includes the coordinate X, the boundary-layer flow is a slowly spatially developing flow except for a special case ($a = 1$). Equations (3.2) and (3.3) are solved by a fourth-order Runge–Kutta procedure and shooting method, and the results are shown in figures 2(*a*) and 2(*b*).

The following forms of disturbance streamfunction and temperature are employed (subscript 1 refers to the normal mode):

$$\psi_1 = 2\sqrt{2}[1+(a-1)\epsilon X]\Psi_1(\eta)\exp[\mathrm{i}(k_1X - \omega_1\tau)], \quad \phi_1 = \Phi_1(\eta)\exp[\mathrm{i}(k_1X - \omega_1\tau)], \tag{3.4}$$

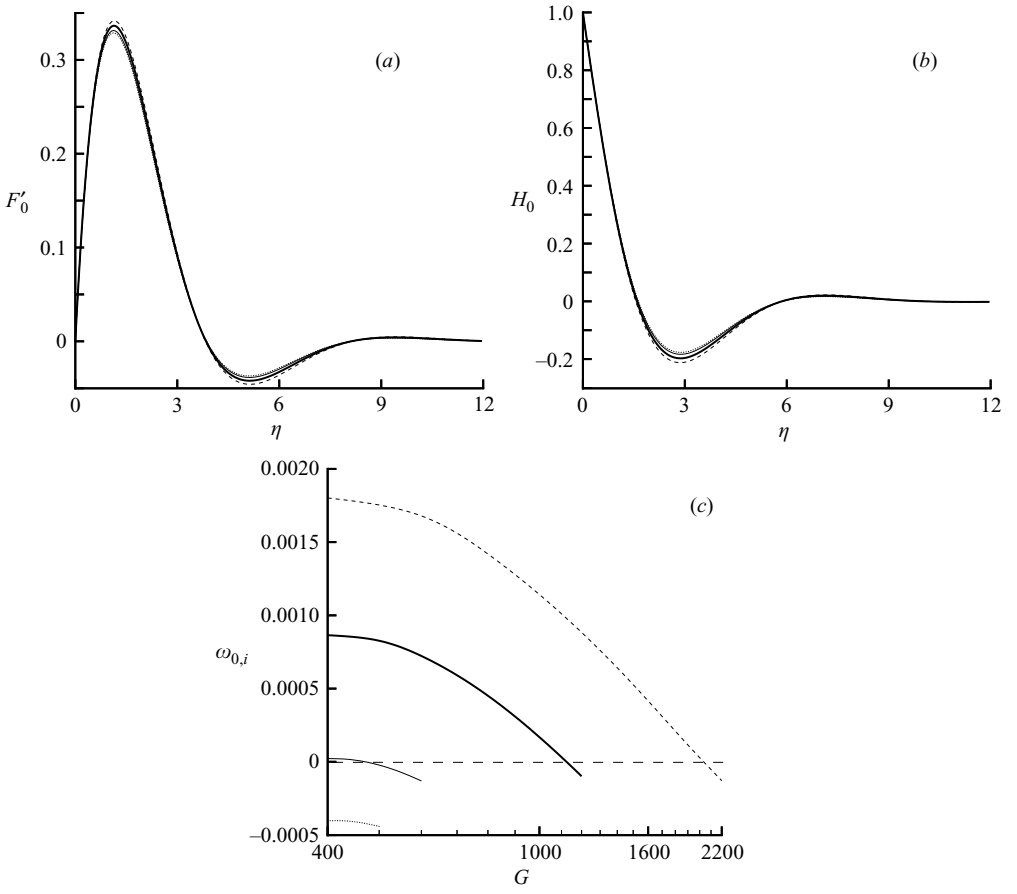

FIGURE 2. (*a*) Vertical velocity, (*b*) temperature profiles of the basic flows and (*c*) modified absolute growth rate for various temperature gradient ratios a for $Gr = 185, a = 0.72$. The dashed line, thick solid line, thin solid line and dotted line correspond to $a = 0.68, 0.7, 0.72$ and 0.73, respectively.

and the Orr–Sommerfeld equation coupled with the energy equation can be obtained according to stability theory:

$$\left.\begin{aligned} &\left(\Psi_1'' - k^2\Psi_1\right)F_0' - \frac{\omega}{k} - F_0'''\Psi_1 = \frac{1}{\mathrm{i}kG}\left[\Psi_1'''' - 2k^2\Psi_1'' + k^4\Psi_1 + \Phi_1'\right], \\ &F_0' - \frac{\omega}{k}\Phi_1 - H_0'\Psi_1 = \frac{1}{\mathrm{i}kGPr}\left(\Phi_1'' - k^2\Phi_1\right) - \frac{4}{\mathrm{i}kG}\Phi_1', \end{aligned}\right\} \tag{3.5}$$

with the boundary conditions

$$\Psi_1(0) = \Psi_1'(0) = \Phi_1(0) = \Psi_1'(\infty) = \Phi_1(\infty) = 0, \tag{3.6}$$

where $G = 2\sqrt{2}Gr[1 + (a-1)\epsilon X]$, $k = \sqrt{2}k_1$ and $\omega = \omega_1/(\sqrt{2}[1 + (a-1)\epsilon X])$. The modified Grash of number G, wavenumber k and frequency ω provide general measures for instability properties. In order to deduce equations (3.5) and (3.6) some additional terms are ignored as $G^{-1} \ll 1$ is assumed. This condition is satisfied well in all instability problems discussed later.

The coupled disturbance equations (3.5) and (3.6) are discretized with a fourth-order finite difference scheme at uniformly distributed points in the η interval, and a

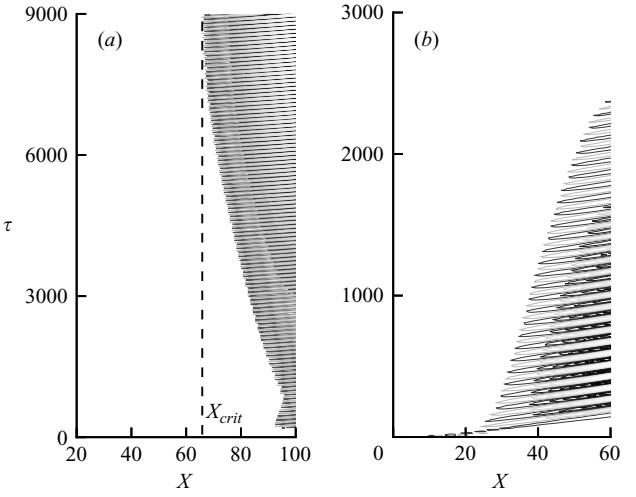

FIGURE 3. Spatio-temporal diagrams of v at $\eta = 2$ for $Gr = 185$ and $a = 0.72$: (a) globally unstable case with contour spacing 0.0032, (b) convectively unstable case with contour spacing 0.00076. The vertical dashed line indicates the theoretical position X_{crit} for marginal absolute instability. The (X_0, η_0) of initial disturbances for (a) and (b) are (60, 1.3) and (10, 1.3), respectively.

fully spatio-temporal stability analysis is carried out in order to compare with direct numerical simulation results. For details of the solution methods refer to Tao & Zhuang (2000) and Tao *et al.* (2004*b*).

According to the Briggs–Bers criterion which is associated with a zero-group-velocity condition: $\mathrm{d}\omega/\mathrm{d}k(k_0) = 0$ and $\omega_0 = \omega(k_0)$, a flow is locally convectively unstable when the modified growth rate $\omega_{0,i} < 0$ and locally absolutely unstable when $\omega_{0,i} > 0$; $\omega_{0,r}$ is the modified absolute frequency. Furthermore, a finite absolutely unstable domain will lead to global instability for spatially developing flows provided that the domain is sufficiently long (Chomaz 2005). As shown in figure 2(c), decreasing a will increase the critical G_{crit} where $\omega_{0,i} = 0$ for the present boundary layers. It is a demanding task to investigate numerically the full three-dimensional parameter space spanned by the parameters G, a, Pr and we shall restrict the discussion to several examples with $Pr = 0.35$ and $a = 0.72$, where the critical Grashof numbers for convective/absolute instability transition are low enough for numerical simulation, and the convectively unstable regions are long enough to show clearly the trailing front separating the base-state region from the bifurcated-state domain. The Prandtl number's effect on the local convective/absolute instability transitions has been investigated theoretically in Tao *et al.* (2004*a*). Since Gr is chosen and fixed in numerical simulations, the modified Grashof number G decreases as X increases in the downstream direction. This feature is helpful for us to study the spatio-temporal properties at G_{crit} as we can set the inlet and the outlet in the convectively unstable and the absolutely unstable regions, respectively.

4. Results

The spatio-temporal diagrams in figure 3 illustrate the evolution of two initial perturbations in the boundary-layer flows. Note that $G_{crit} = 471.07$ (figure 2c) and the corresponding $X_{crit} = 65.9$ for $a = 0.72$ and $Gr = 185$. The early-time evolution

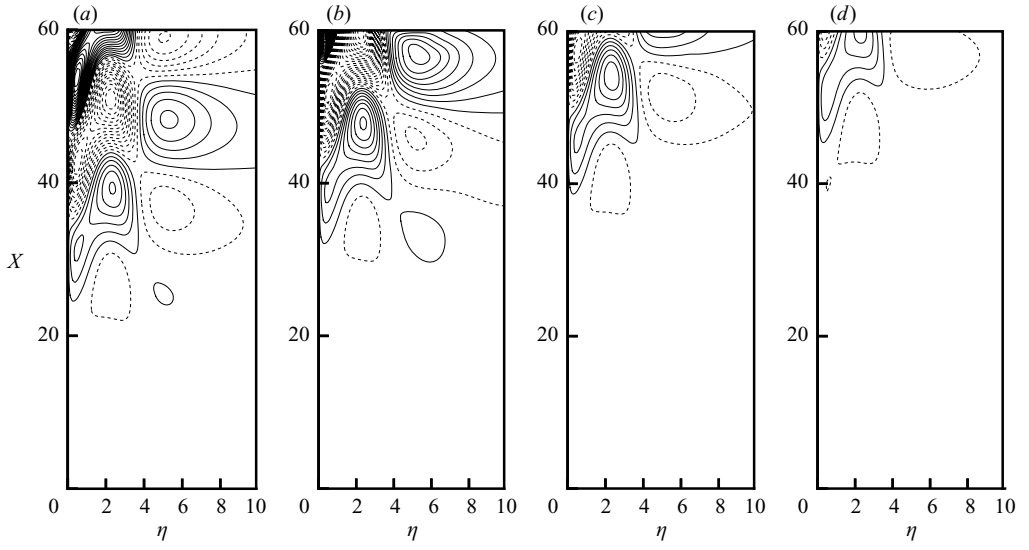

FIGURE 4. Flow field of convectively unstable case: contour lines of u for $Gr = 185$ and $a = 0.72$. Contour spacing is 0.00051. Obtained at (a) $\tau = 200$, (b) 800, (c) 1400 and (d) 2000. Solid (dotted) lines indicate positive (negative) values of u. (X_0, η_0) of initial disturbance is (10, 1.3).

is similar in both cases: the generated wave packet rapidly grows and saturates as time increases. The difference between these cases is that the trailing front propagates upstream in the locally absolutely unstable domain ($X > X_{crit}$ in figure 3a) and is blocked around the critical position X_{crit} of marginal absolute instability, whereas it moves downstream in the convectively unstable region $X < X_{crit}$ (figure 3b). Therefore, this result confirms the prediction of the existence of global instability in flat-plate boundary-layer flows (Tao *et al.* 2004a). The evolution in figure 3(a) is slower than in figure 3(b) since the closer to the absolute threshold, the smaller the speed of the trailing front and the longer the time needed for the unstable flow to be saturated.

The time series of the spatially evolving disturbance field are shown in figure 4 and figure 5. It is seen that the initial impulse perturbation induces a front of finite-amplitude waves whose amplitudes increase in the downstream direction but decrease with time. As a result, the front moves downstream and the flow relaxes to zero for the convectively unstable case (figure 4). On the contrary, the amplitudes of the globally unstable waves increase with time until the front reaches its saturated state at the critical position (figure 5). It is also shown in figure 5 that the domain upstream of the dashed line remains unperturbed except for the upstream neighbourhood of the trailing front, where the disturbance amplitude decreases in the upstream direction due to the convectively unstable property. This fact is used to examine numerically the critical position for global instability.

We check the time series of the disturbance velocity at a fixed point which is in the convectively unstable region but very close to the critical position. By increasing gradually the length L of computational domain for given values of Gr and a, the maximum amplitude of the disturbance velocity at the fixed point decreases with time when the original domain is entirely convectively unstable or increases when the globally unstable region is included near the outlet. As shown in figure 6(a) the flow at the outlet of the computational domain is not absolutely unstable until $L = 66.5$. Therefore, the critical position for global instability X_{crit} is between

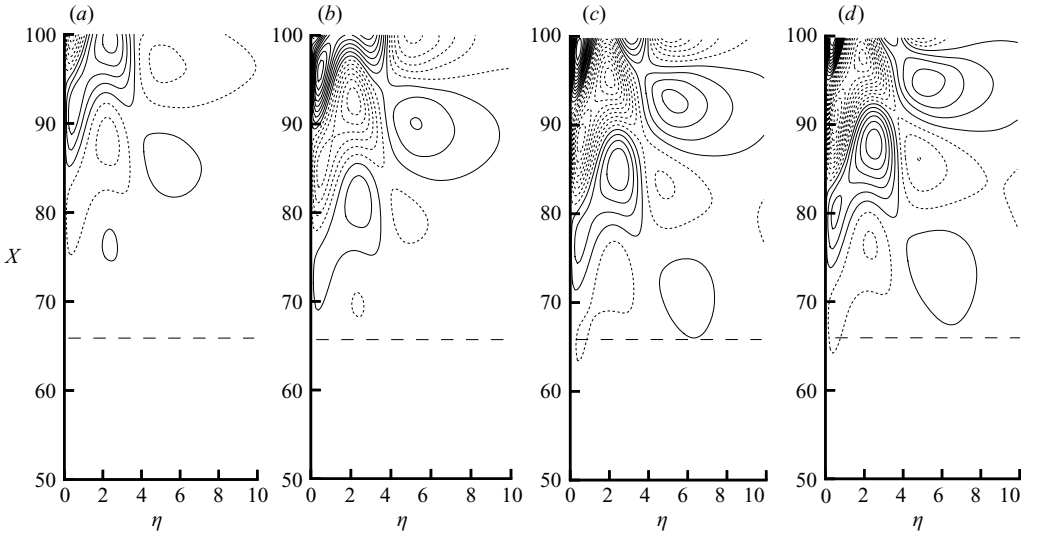

FIGURE 5. Flow field of globally unstable case: Contour lines of u for $Gr = 185$ and $a = 0.72$. Contour spacing is 0.0068. Obtained at (*a*) $\tau = 5000$, (*b*) 7000, (*c*) 9000 and (*d*) 11000. The dashed line indicates the theoretical position for marginal absolute instability. Solid (dotted) lines indicate positive (negative) values of u. (X_0, η_0) of initial disturbance is (60, 1.3).

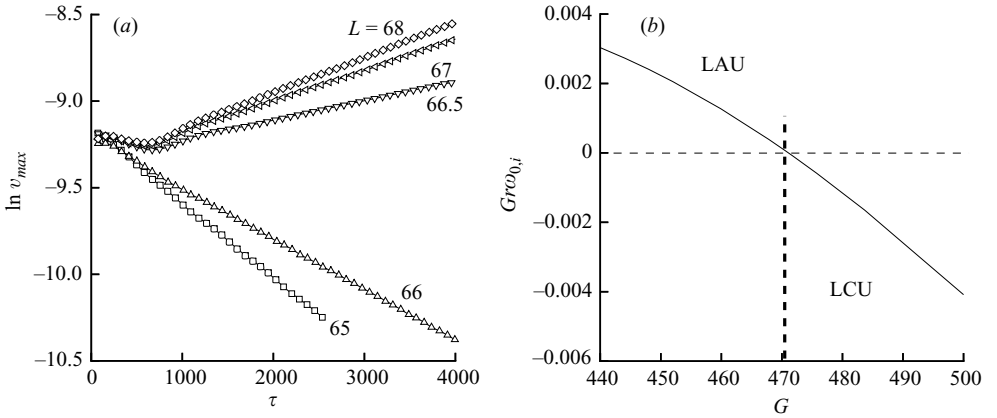

FIGURE 6. (*a*) Time dependence of the maximum amplitude of $v(X = 60, \eta = 2)$ calculated at different lengths L of the computational domain for $Gr = 185, a = 0.72$. (*b*) The modified absolute growth rate as a function of modified Grashof number G. The vertical dashed line indicates the critical G_{DNS} of global instability obtained from direct numerical simulation. LAU: locally absolutely unstable, LCU: locally convectively unstable.

(66, 66.5). The corresponding modified critical Grashof number G_{DNS}, shown in figure 6(*b*) as a vertical dashed line, agrees very well with the marginal G_{crit} for local absolute instability. The relative difference between the DNS and theory is: $|G_{crit} - G_{DNS}|/G_{crit} < 0.101\%$. Therefore, the position of the trailing front is determined by its local dispersion relation, though the initial temporal growth rates of waves near the front are also affected by downstream unstable modes due to its global instability characteristics.

A key issue for global instability is the global frequency selection criterion. Time series are recorded at positions close to the front and downstream far from the front

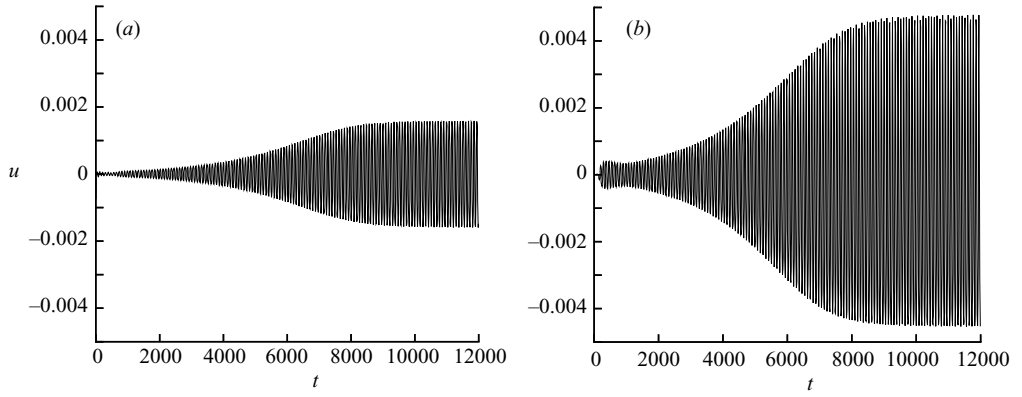

FIGURE 7. Time series of disturbance velocity u at (a) $X = 68$, $\eta = 2$ and (b) $X = 100$, $\eta = 2$ for $Gr = 185$, $a = 0.72$ and $L = 100$.

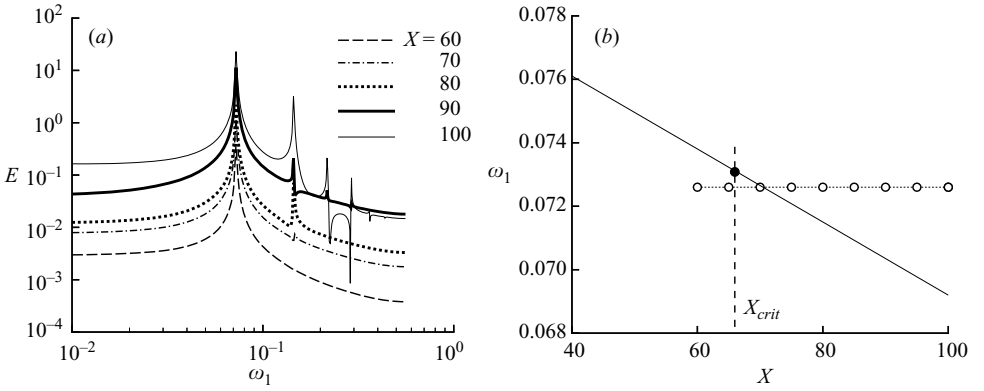

FIGURE 8. (a) Power spectra of u at different streamwise positions with $\eta = 2$. (b) Local absolute frequency as a function of streamwise coordinate X for $Gr = 185$, $a = 0.72$ and $L = 100$. The circles indicate the dominant frequencies obtained from direct numerical simulations and the black point represents the marginal absolute frequency.

(figure 7). It is shown that the disturbances, whose amplitudes increase exponentially in the early stage, reach saturated periodic oscillating states at $\tau = 10000$. The corresponding spectrum analysis is also carried out to analyse this synchronized behaviour of the flow (figure 8a). Inspection of these spectra demonstrates that the globally unstable region is turned into an oscillating state with a global fundamental frequency $\omega_{1,DNS}$ and its harmonics. Figure 8(b) shows that this global frequency stays constant in the downstream direction and is in good agreement with the marginal absolute frequency $\omega_{1,crit} = \omega_1(X_{crit})$ deduced from the local linear dispersion relation based on unperturbed basic flow: the difference is $|\omega_{1,crit} - \omega_{1,DNS}|/\omega_{1,crit} = 0.68\%$. However, note that the consistency between the DNS and theory becomes worse when Gr decreases, as shown in figure 9, because smaller Gr leads to larger $(a-1)\varepsilon$ which represents stronger non-parallelism in the flow field.

5. Concluding discussion

A buoyancy-driven flow near a vertically heated flat plate immersed in a thermally stratified medium is studied numerically and theoretically. In contrast to previous

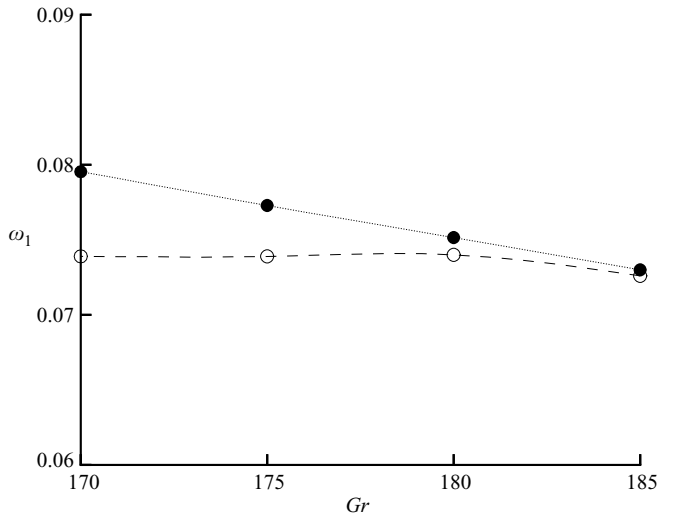

FIGURE 9. Global frequency as a function of the Grashof number Gr for $a = 0.72$. ○ and ● represent the global frequencies obtained from direct numerical simulations and the marginal absolute frequencies, respectively.

flat-plate boundary-layer flows, in the present model nonlinear global modes in the form of self-sustained oscillations with well-defined frequency are identified. The trailing front, separating the convectively unstable domain from the saturated oscillating state, is determined by the marginal absolute instability. The nonlinear global frequency is just the marginal absolute frequency deduced from the local linear dispersion relation.

Such a boundary-layer flow could serve as a model for the study of the laminar–turbulent transition of globally unstable flow and offers several advantages. First, it has a free trailing front selected naturally by the flow, while for most other open shear flows, for instance the cylinder wake which is the most popular model, the upstream threshold of absolute instability is a solid wall. Secondly, it is found that the strong non-parallelism in cylinder wakes may account for the discrepancy between onset of absolute instability and onset of global instability (Pier 2002), while for the present model its non-parallelism is characterized by $(a - 1)\varepsilon$, which is much smaller than unity in most cases. Finally, in contrast to the flow produced by a rotating disk where a sharp turbulence transition occurs owning to the coincidence of the secondary absolute instability and the primary instability (Pier 2003), the present globally unstable flow (figure 7) reaches a saturated state at appropriates parameters. This is very convenient and helpful in the study of the sequence of bifurcation (Busse 2003) leading to turbulence. In our calculation, it is also found that the secondary instability will occur when the globally unstable domain is large enough, and its spatio-temporal characteristics will be a future research topic.

This work has been supported by the Alexander von Humboldt Foundation. Suggestions and advice from Friedrich H. Busse are gratefully acknowledged.

REFERENCES

BERS, A. 1983 Space-time evolution of plasma instabilities-absolute and convective. In *Handbook of Plasma Physics* (ed. M. Rosenbluth & R. Sagdeev), pp. 451–517. North-Holland.

Brandt, L., Cossu, C., Chomaz, J. M., Huerre, P. & Henningson, D. S. 2003 On the convectively unstable nature of optimal streaks in boundary layers. *J. Fluid Mech.* **485**, 221–242.

Briggs, R. 1964 *Electron-stream Interaction with Plasmas*. MIT Press.

Busse, F. H. 2003 The sequence-of-bifurcations approach towards understanding turbulent fluid flow. *Surveys Geophys.* **24**, 269–288.

Chomaz, J. M. 2003 Fully nonlinear dynamics of parallel wakes. *J. Fluid Mech.* **495**, 57–75.

Chomaz, J. M. 2005 Global instabilities in spatially developing flows: non-normality and nonliearity. *Annu. Rev. Fluid Mech.* **37**, 357–392.

Chorin, A. J. 1967 A numerical method for solving incompressible viscous flow problems. *J. Comput. Phys.* **2**, 12–26.

Couairon, A. & Chomaz, J. M. 1997*a* Absolute and convective instabilities, front velocities and global modes in nonlinear systems. *Physica* D **108**, 236–276.

Couairon, A. & Chomaz, J. M. 1997*b* Pattern selection in the presence of a cross flow. *Phys. Rev. Lett.* **79**, 2666–2669.

Couairon, A. & Chomaz, J. M. 1999*a* Fully nonlinear global modes in slowly varying flows. *Phys. Fluids* **11**, 3688–3703.

Couairon, A. & Chomaz, J. M. 1999*b* Primary and secondary nonlinear global instability. *Physica* D **132**, 428–456.

Dee, G. & Langer, J. 1983 Propagating pattern selection. *Phys. Rev. Lett.* **50**, 383–386.

Delbende, I. & Chomaz, J. M. 1998 Nonlinear convective/absolute instabilities of parallel two-dimensional wakes. *Phys. Fluids* **10**, 2724–2736.

Gaster, M. & Grant, I. 1975 An experimental investigation of the formation and development of a wave packet in a laminar boundary layer. *Proc. R. Soc. Lond.* A **347**, 253–269.

Gebhart, B., Jaluria, Y., Mahajan, R. & Sammakia, B. 1988 *Buoyancy-induced Flows and Transport*. Hemisphere.

Högberg, M. & Henningson, D. 1998 Secondary instability of cross-flow vortices in falkner-skan-cooke boundary layers. *J. Fluid Mech.* **368**, 339–357.

Huerre, P. 2000 Open shear flow instabilities. In *Perspectives in Fluid Dynamics* (ed. G. Batchelor, H. Moffatt & M. Worster), pp. 159–229. Cambridge University Press.

Koch, W. 1985 Local instability characteristics and frequency determination on self-excited wake flows. *J. Sound Vib.* **99**, 53–83.

Koch, W. 2002 On the spatio-temporal stability of primary and secondary crossflow vortices in a three-dimensional boundary layer. *J. Fluid Mech.* **456**, 85–111.

Krizhevsky, L., Cohen, J. & Tanny, J. 1996 Convective and absolute instabilities of a buoyancy-induced flow in a thermally stratified medium. *Phys. Fluids* **8**, 971–977.

Marquillie, M. & Ehrenstein, U. 2003 On the onset of nonlinear oscillations in a separating boundary-layer flow. *J. Fluid Mech.* **490**, 169–188.

Monkewitz, P. A. & Nguyen, L. 1987 Absolute instability in the near-wake of two-dimensional bluff bodies. *J. Fluids Struct.* **1**, 165–184.

Monkewitz, P. A. & Sohn, K. D. 1986 Absolute instability in hot jets and their control. *AIAA Paper* 86–1882.

Peyret, R. & Taylor, T. D. 1990 *Computational Methods for Fluid flow*. Springer.

Pier, B. 2002 On the frequency selection of finite-amplitude vortex shedding in the cylinder wake. *J. Fluid Mech.* **458**, 407–417.

Pier, B. 2003 Finite-amplitude crossflow vortices, secondary instability and transition in the rotating-disk boundary layer. *J. Fluid Mech.* **487**, 315–343.

Pier, B., Huerre, P., Chomaz, J. M. & Couairon, A. 1998 Steep nonlinear global modes in spatially developing media. *Phys. Fluids* **10**, 2433–2435.

Prandtl, L. 1952 *Essentials of Fluid Dynamics*. London: Blackie.

Tao, J., Le Quéré, P. & Xin, S. 2004*a* Spatio-temporal instability of the natural-convection boundary layer in thermally stratified medium. *J. Fluid Mech.* **518**, 363–379.

Tao, J., Le Quéré, P. & Xin, S. 2004*b* Absolute and convective instabilities of natural convection flow in boundary-layer regime. *Phys. Rev.* E **70**, 066311.

Tao, J. & Zhuang, F. 2000 The absolute and convective instabilities of the natural convection in vertical heated slot. *Phys. Rev.* E **62**, 7957–7960.